Ultrafast Fetal MRI and Prenatal Diagnosis

By Anne M. Hubbard
Philadelphia, Pennsylvania

Improvements in magnetic resonance imaging (MRI) technology continue to provide faster scan times and higher resolution increasing the applications for fetal imaging. MRI is an adjunct to good prenatal ultrasound scan (US). It provides significant additional information that improves diagnostic accuracy in evaluation of the fetal brain, spine, neck, chest, abdomen, and urinary tract. MRI provides important anatomic information that helps in planning delivery and surgical procedures.

ULTRAFAST MAGNETIC RESONANCE IMAGING (MRI) has been shown to provide detailed and reproducible fetal anatomy.[1,2] MRI is most useful in evaluation of abnormalities of the fetal brain, neck, chest, and abdomen. It is difficult to adequately evaluate the fetus before 18 weeks' gestation because of the small size of the fetus.

Safety is paramount in evaluating the fetus. No known harmful effects to the developing human fetus have been documented at field strengths of 1.5 Tesla or less. However, safety has not been proven. Animal studies have been performed looking at the effects of radio frequency fields on fetal development.[3] Even at high levels, above permissible human guidelines, consistent morphologic or organ abnormalities have not been identified. In utero exposure to echo-planar imaging has not shown any effect on fetal growth.[4] A 2-year follow-up study of children who underwent imaging in utero showed no demonstrable increase in disease occurrence.[5]

CENTRAL NERVOUS SYSTEM

Ultrasound Scan (US) is the primary modality for fetal evaluation. There are pitfalls in the evaluation of the fetal brain and spine with US. The normal and abnormal appearance of the brain on US is based on the ability to obtain specific images of the cerebrum, cerebellum, and spine. Maternal obesity, oligohydramnios, or poor fetal position may cause inability to obtain adequate US images. MRI is less affected by these factors. MRI has been shown to augment US diagnosis of Central nervous system (CNS) abnormalities. MRI has changed the diagnosis in 40% of fetuses and changed the management in 46%.[6,7]

MRI significantly affects the evaluation of the developing fetal brain. MRI shows changes in the developing brain owing to neuronal migration, gyral formation, and myelination. In vitro MRI shows specific patterns of growth that correlate with anatomic changes seen in pathologic specimens.[8] At 16 to 20 weeks, the cerebral surface is relatively smooth, with only minimal infolding of the sylvian fissures (Figs 1 and 2). MRI shows increased sulcation with maturation.[9,10] The appearance of specific sulci can be used to estimate gestational age. The in utero MRI visualization of specific sulci lags 2 to 3 weeks behind pathologic specimens.[11] MRI shows a multilayered pattern of brain parenchyma corresponding to cellular migration. MRI depicts signal changes corresponding to increased cellularity and the evolving process of myelination.[12]

Abnormalities of neuronal migration were previously felt to be rare. However, they are seen in greater than 20% of CNS anomalies identified on postnatal MRI.[13] They may be isolated or in association with other cerebral anomalies. Prenatal MRI visualizes areas of heterotopic brain in 54% of third trimester fetuses with a postnatal diagnosis of migrational disorder. Third trimester MRI shows 80% of lissencephaly, 73% of polymicrogyria, and 100% of schizencephaly.[14] Polymicrogyria has been documented in utero.[6,13] Polymicrogyria may result from injury to normal cellular interactions at the external limiting membrane, the pial-glial barrier. The most common form of injury is ischemia.[13] Schizencephaly is a migration anomaly characterized by gray matter–lined clefts extending from the ventricle to the cortical surface. The lips of the clefts may be fused or separate. Prognosis is related to the amount of cortex involved. The cause may be genetic or ischemic. The defects are better visualized and characterized with MRI.[15]

Ventriculomegaly is the most common referral for MRI evaluation of the fetal CNS. Mild to moderate enlargement of the ventricles is associated frequently with other anomalies.[16] Associated CNS abnormalities have been diagnosed in 84% of fetuses with hydrocephalus. Outcomes of fetuses born with hydrocephalus are discouraging with normal intelligence in only 50% to 60%. In cases of rapidly progressive severe hydrocephalus, there is invariably poor postnatal outcome.[17] Compared with US, MRI more accurately shows the cause of

From the Department of Radiology, The Children's Hospital of Philadelphia and The University of Pennsylvania School of Medicine, Philadelphia, PA.

Address reprint requests to Anne M. Hubbard, MD, The Children's Hospital of Philadelphia, Department of Radiology, 34th St and Civic Center Boulevard, Philadelphia, PA 19104.

1055-8586/03/1203-0000$30.00/0
doi:10.1016/S1055-8586(03)00031-3

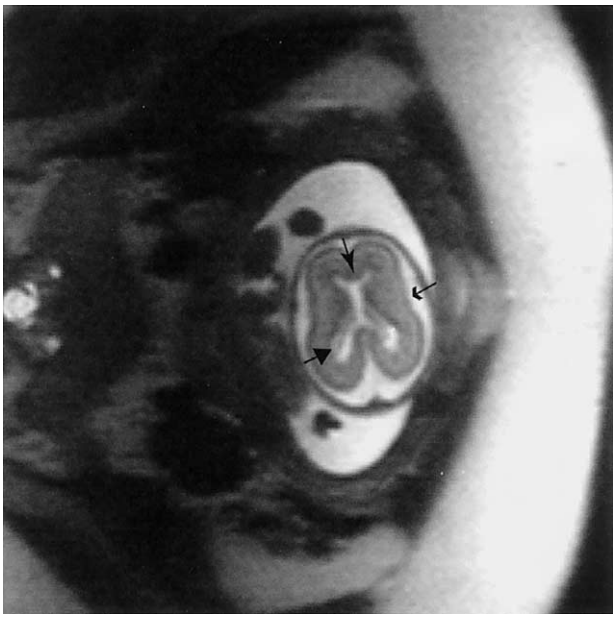

Fig 1. Normal brain in a fetus at 20 weeks' gestation. Axial T_2-weighted image shows normal ventricular size. There is a discrete low signal intensity periventricular zone (large arrow) and low signal cortical zone (small arrow). The cortical surfaces are smooth. The intermediate zone is homongenous. The corpus callosum is seen anteriorly (curved arrowhead).

Fig 2. Normal brain in a fetus at 21 weeks' gestation. Sagittal T_2-weighted image shows a well-developed corpus callosum (small arrow). The posterior fossa structures are well visualized including the fourth ventricle (curved arrowhead) and the cerebellum (large arrow).

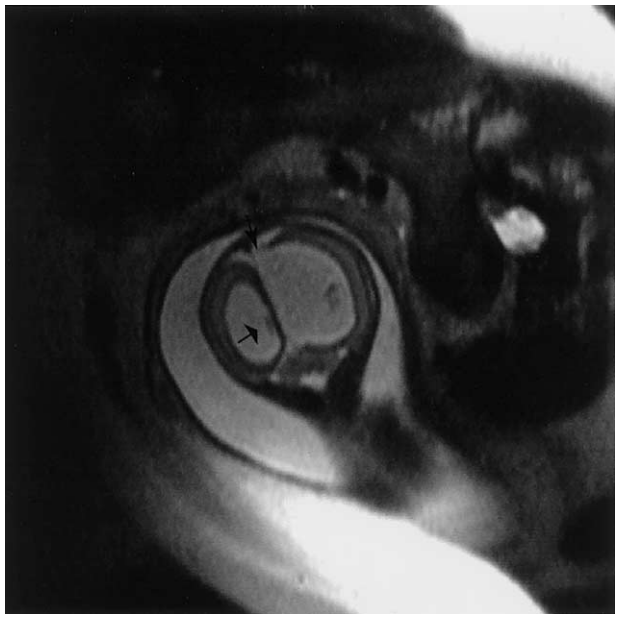

Fig 3. Ventriculomegaly in a fetus at 22 weeks' gestation. Coronal T_2-weighted image shows severe asymmetric ventriculomegaly (short broad arrow). The is obliteration of the extra-axial spaces. There is cortical destruction (curved arrowhead) in the parietal lobe.

ventriculomegaly and identifies associated brain anomalies.[6]

The diagnosis of aqueductal stenosis is made on MRI with demonstration of dilation of the lateral and third ventricles and a normal-size fourth ventricle. There usually is obliteration of the subarachnoid space.[6] Aqueductal stenosis may be congenital or acquired after hemorrhage or infection.

Ventriculomegaly with cerebral atrophy is seen after ischemic or infectious events (Fig 3). There may be unilateral or bilateral enlargement of the ventricles. There may be porencephaly with focal cortical loss and dilation of the ventricle.[18] There is enlargement of the extra-axial spaces with cerebral atrophy. Irregularity of the ventricular surface may follow ischemic or inflammatory insults to the brain (Fig 4).

The frequency of in utero cerebral ischemic injuries is not known. Fourteen percent of perinatal deaths in one study were associated with ischemic changes.[19] Ischemic injury has a variable appearance. The morphology depends on the area affected and the amount of time between the insult and imaging.[20] Findings include ventriculomegaly, microcephaly, hydranencephaly, porencephaly, encephalomalacia, capsular ischemia, and cerebral atrophy. MRI is superior to US in showing these changes (Fig 5).

The corpus callosum is developed by 20 weeks. Abnormalities of the corpus callosum are detected on prenatal MRI. Associated CNS abnormalities have been

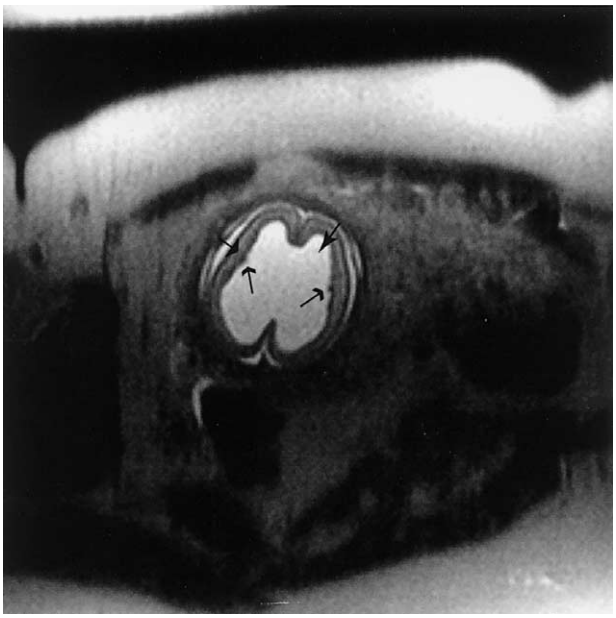

Fig 4. Ventriculomegaly in a fetus at 23 weeks' gestation. Axial T_2-weighted image shows severe ventriculomegaly (curved arrowhead). There is moderate thinning of the cortex (broad arrow). Note the nodularity of the ventricular surfaces (small arrows), which can be seen after infection or ischemia.

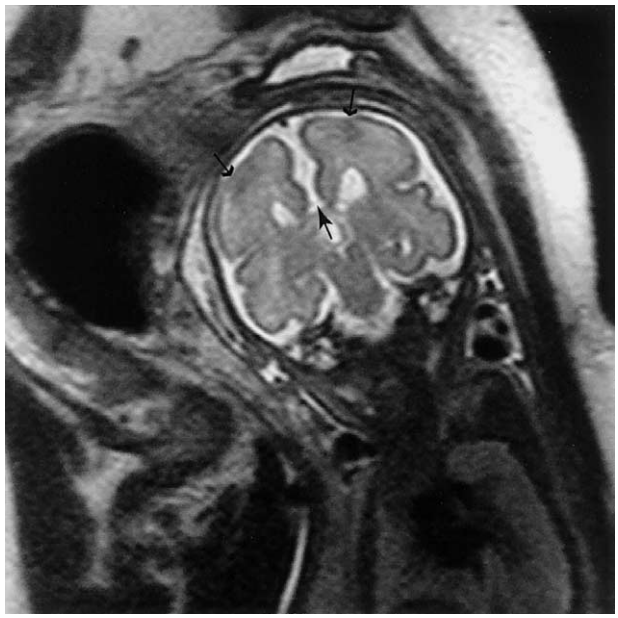

Fig 6. Agenesis of the corpus callosum in a fetus at 27 weeks' gestation. Coronal T_2-weighed image shows lack of normal connecting white matter fibers (curved arrowhead) between the cerebral hemispheres. Also bilateral areas of heterotopic (small arrows) brain in the subcortical area seen as foci of lower signal intensity.

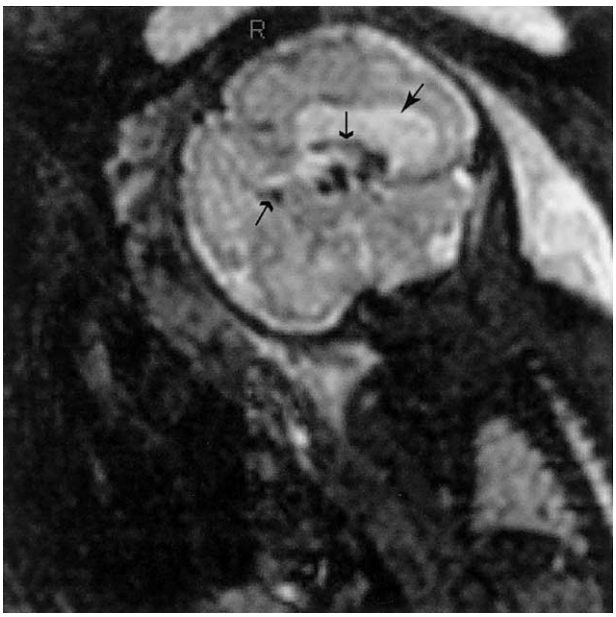

Fig 5. Ventriculomegaly and hemorrhage in fetus at 29 weeks' gestation with a cotwin demise. Axial echo planar (EPI) image shows asymmetric ventriculomegaly (curved arrowhead). There are multiple areas of low signal intensity (short arrows) consistent with periventricular hemorrhage. EPI is very useful to define hemorrhage.

found in 60% of patients with abnormalities of the corpus callosum.[14] The MRI and US appearance of absent corpus callosum is similar with separation of the bodies of the lateral ventricles, upward displacement of the third ventricle, and lack of connecting fibers between the cerebral hemispheres (Fig 6). Partial agenesis of the corpus callosum may be difficult to diagnose on US. MRI shows partial agenesis or thinning of the corpus callosum. Arachnoid cysts occur in the area of the roof of the third ventricle and may be misdiagnosed as agenesis of the corpus callosum. MRI differentiates these lesions by showing the wall of the cyst and a normal corpus callosum.

Holoprosencephaly is a malformation of the prosencephalon with a failure of normal midline cleavage and associated with incomplete midface development. The severe forms, semilobar and alobar holoprosencephaly, are diagnosed easily because of the presence of a monoventricle and obvious fusion of the cerebral hemispheres. MRI is most helpful to distinguish the lobar form of holoprosencephaly from other causes of ventriculomegaly.[14,21] In lobar holoprosencephaly there is a falx and some separation of the cerebral hemispheres. In all forms of holoprosencephaly there is some fusion of the thalami and rostral portion of the brain.

Tuberous sclerosis (TS) is an autosomal dominant disorder that affects brain, heart, skin, kidneys, and other organs. Mental retardation and seizures may be mild or

Fig 7. Arachnoid cyst in the posterior fossa in a fetus at 26 weeks' gestation. Axial T_2-weighted image shows a cyst (curved arrowhead) in the left side of the posterior fossa with compression and distortion of the shape of the cerebellar hemisphere (small arrow).

severe. Prenatal diagnosis is based on finding cardiac rhabdomyomas. The diagnostic accuracy increases with increasing numbers of cardiac rhabdomyomas; 30% incidence with one myoma and 80% with 2 or more.[22] Approximately 50% of patients with postnatal diagnosis of TS have cardiac rhabdomyomas; however, most are not present on 20-week gestation US. MRI provides better definition of the periventricular and subcortical brain than US. Subependymal tubers in the brain have been seen at 21 weeks. The tuber is low signal on T_2-weighted images and high signal on T_1-weighted images. The lesion may be seen as a defect in the contour of the ventricular wall. Heterotopic brain may be identified in the subcortical region (Fig 6). Hamartomas may not develop until after birth making screening difficult.[22]

Many abnormalities of the posterior fossa carry a poor prognosis. The evaluation of the posterior fossa on US depends on a single angled axial view through the cerebellar hemispheres and region of the cisterna magna. Dandy-Walker malformation, Dandy-Walker variant, and mega cisterna magna represent a spectrum of developmental abnormalities. Mega cisterna magna has an intact cerebellar vermis and fourth ventricle with an enlarged posterior fossa cerebrospinal fluid space. In Dandy-Walker malformation there is agenesis of the inferior vermis, cystic dilation of the fourth ventricle communicating with the cisterna magna, and enlargement of the posterior fossa with upward displacement of the tentorium.[14] Dandy-Walker variant consists of varying degrees of hypoplasia of the inferior cerebellar vermis with cystic dilation of the fourth ventricle but without enlargement of the posterior fossa. Isolated mild vermian hypoplasia probably has a good outcome. Supratentorial malformations are found in 68% of Dandy-Walker malformations. Hydrocephalus usually develops postnatally. MRI significantly improves visualization of the posterior fossa.[23] MRI differentiates posterior fossa arachnoid cysts from abnormalities of vermian development (Fig 7).

Abnormalities of the brain are associated with spinal dysraphism. The classic findings of a Chiari II malformation are seen with MRI including a small cone-shaped posterior fossa, obliteration of the fourth ventricle, and downward herniation of the cerebellar tonsils (Fig 8).[6] There may be ventriculomegaly. MRI of open spina bifida shows a cystic lesion usually in the lumbosacral spine with widening of the lamina. There may be a simple meningocele or neural elements within the sac.[24] US is more accurate in determining the defect level and evaluating small sacral lesions.[25]

In utero repair of myelomeningocele has been performed.[26] Findings after in utero surgery show improvement in hindbrain herniation with reaccumulation of cerebral spinal fluid within the posterior fossa (Fig 9).

Sacrococcygeal tumors (SCT) may be diagnosed in utero. SCT arise from the coccyx and are classified according to the amount of extra-or intrapelvic compo-

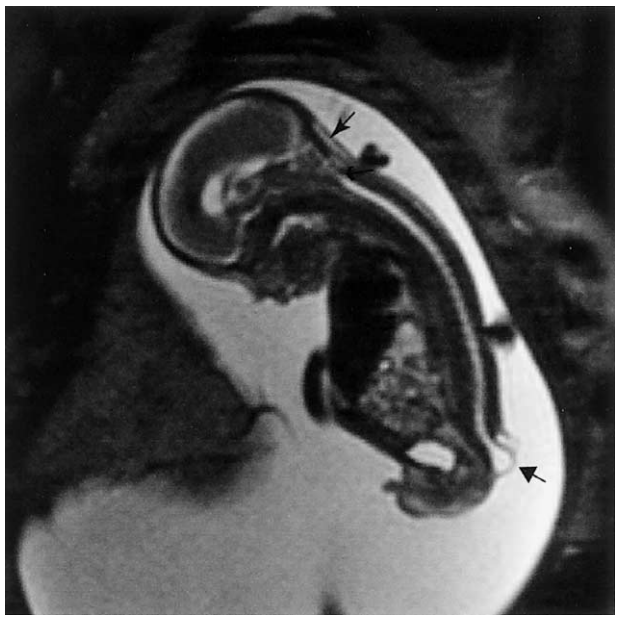

Fig 8. Myelomeningocele in a fetus at 22 weeks' gestation. Sagittal T_2-weighted image shows a small cone-shaped posterior fossa (curved arrowhead) with downward herniation of the cerebellar tonsils (small arrow). There is a well-defined low lumbar sac (large arrow) containing neural elements.

Fig 9. Myelomeningocele 4 weeks post–in utero repair. Axial T_2-weighted image of the posterior fossa shows reversal of Chiari II malformation with a normal size and shape of the fourth ventricle (curved arrowhead), CSF in the posterior fossa (small arrow), and normal shape of the cerebellar hemisphere.

nent.[27] Type I is external with a small presacral component. Type II is predominantly external with a small intrapelvic component. Type III has a small extrapelvic component but is predominantly intrapelvic with intraabdominal extension. Type IV is within the pelvis and abdomen and is frequently malignant (Fig 10). SCT may be cystic or solid. SCT is associated frequently with polyhydramnios. The larger the solid component the more likely the lesion will have increased vascularity. There may be associated hydrops. US better shows increased flow in the fetal aorta, inferior vena cava (IVC), and increased fetal cardiac output. Poor outcome has been related to the degree of increased vascularity seen in solid lesions.[28] MRI correlates with US in evaluating the size of the tumor as well as solid versus cystic components. MRI better defines intraspinal and intrapelvic extension of the tumor.[29] MRI differentiates tumors that are predominantly cystic from sacral myelomeningocele.

NECK

Fetal neck masses are uncommon but are important to identify because they may cause life-threatening airway obstruction at birth. The most common neck masses are cystic hygromas, teratomas, and goiters. MRI characterizes the lesion and defines the relationship to the airway and major neck vessels.[30]

Teratomas usually occur in the midline. MRI shows a mixed solid and cystic mass with variable signal intensity (Fig 11),[31] Teratomas, occasionally are solitary thick-walled cysts. Calcifications are seen frequently in teratomas, which are better shown with US. Large teratomas may cause hypoplasia of the facial bones.

There are various types of cystic hygroma, a congenital failure of normal cannulation of the lymphatic system. Lesions occurring early in the second trimester in the posterior nuchal region are associated frequently with hydrops and chromosomal abnormalities. Lymphangiomas occurring in the anterior neck or retropharyngeal area usually are isolated abnormalities. There is a tendency for lymphangioma to violate tissue planes, surround neurovascular structures, and extend into the mediastinum. On MRI, these tumors are predominantly cystic with fluid layers in the cysts (Fig 12).[30]

Congenital high airway obstruction syndrome (CHAOS) is caused by intrinsic obstruction of the airway preventing flow of alveolar fluid out of the lungs. The causes include laryngotracheal atresia, laryngeal web, and laryngeal cyst. Large fluid-filled echogenic lungs, dilation of the tracheobronchial tree, and eversion of the diaphragm are seen on US. There usually is hydrops. CHAOS may be misdiagnosed as bilateral congenital cystic adenomatoid malformation. T_2-weighted MRI

Fig 10. Sacrococcygeal teratoma in a fetus at 27 weeks' gestation. Sagittal T_2-weighted image shows a large heterogeneous solid mass (curved arrowheads) externally and in the abdomen consistent with a stage III SCT. Tumor is seen at the tip of the coccyx (short broad arrow) extending into the spinal canal. The symphysis pubis is anterior (small arrow) There is superior displacement and enlargement of the liver (large arrow). The heart (double arrow) is enlarged. There is oligohydramnios.

Fig 11. Cervical teratoma in fetus at 33 weeks' gestation. Sagittal T_2-weighted image shows a large mixed signal intensity solid mass (curved arrowhead). There is elevation of the tongue (small arrow). There is marked distortion of the position of the piriform sinus and epiglottis (double arrowhead). There is severe compression of the trachea (short broad arrowhead).

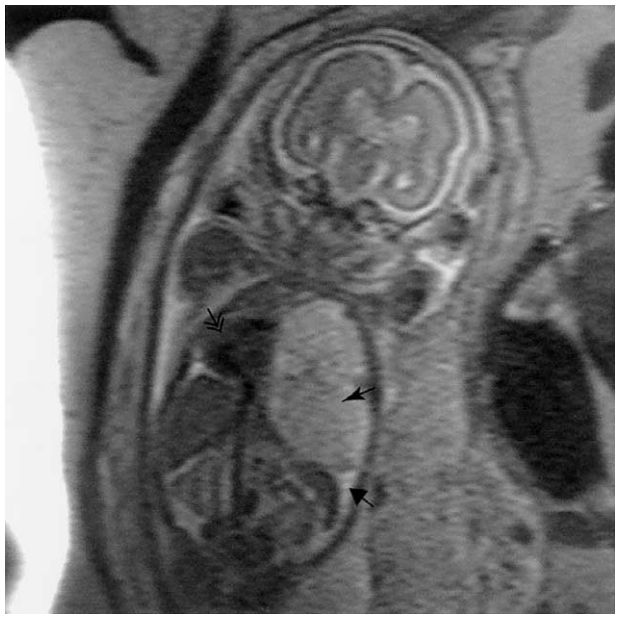

Fig 13. Cystic adenomatoid malformation of the lung in a fetus at 22 weeks' gestation. Coronal T2-weighted image shows a large heterogeneous high signal intensity mass (curved arrowhead) in the left chest with displacement in the heart (double arrow). There is ascites (large arrow).

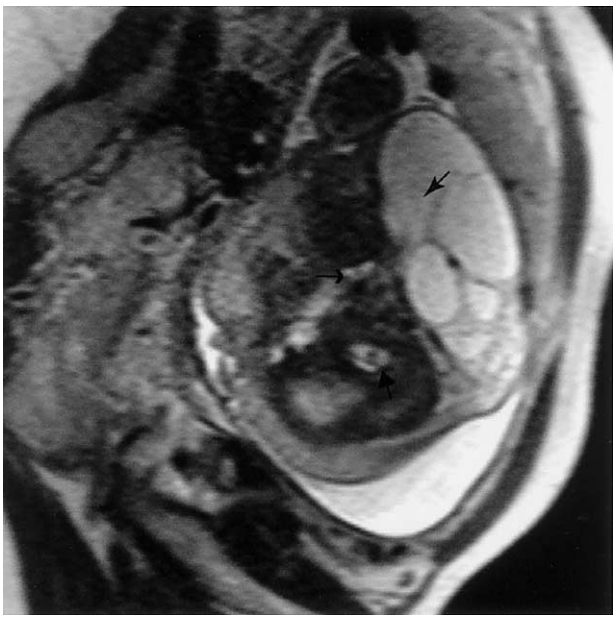

Fig 12. Cervical lymphangioma in a fetus at 33 weeks' gestation. Axial T_2-weighted image at the base of the skull shows the cervical cord (large arrow). There is a large multiseptated cystic mass (curved arrowhead) in the left side of the neck with displacement but no significant compression of the oral pharyngeal airway (small arrow).

shows large, homogeneous, very high signal intensity lungs and a dilated fluid-filled tracheobronchial tree confirming the diagnosis.[30]

CHEST

The most important determinate of fetal survival after birth is adequate development of the lungs. The bronchi and bronchioles are developed by 16 to 20 weeks gestational age with the appearance of a significant number of alveolar ducts and blood vessels by 16 to 24 weeks gestation. The normal fetal lung on T_2-weighted images is homogeneous with moderate signal intensity relative to muscle.[32] Echo-planar imaging showed exponential growth of the lungs with increasing gestational age.[33] MRI changes in the properties of the fetal lungs have been seen with maturation with progressive decrease in T_1 signal and increase in T_2 signal.[34]

The most common fetal chest masses are congenital cystic adenomatoid malformation (CCAM), bronchopulmonary sequestration (BPS), fetal hydrothorax (FHT), and congenital diaphragmatic hernia (CDH). CCAM is an uncommon lesion characterized by a multicystic mass of pulmonary tissue with an abnormal proliferation of bronchiolar structures that connects to the normal bronchial tree. The vascular supply is from the pulmonary artery and drains via the pulmonary veins. The appearance of these tumors on MRI is variable depending on whether they are micro- or macrocytic.[32] Type 1 micro-

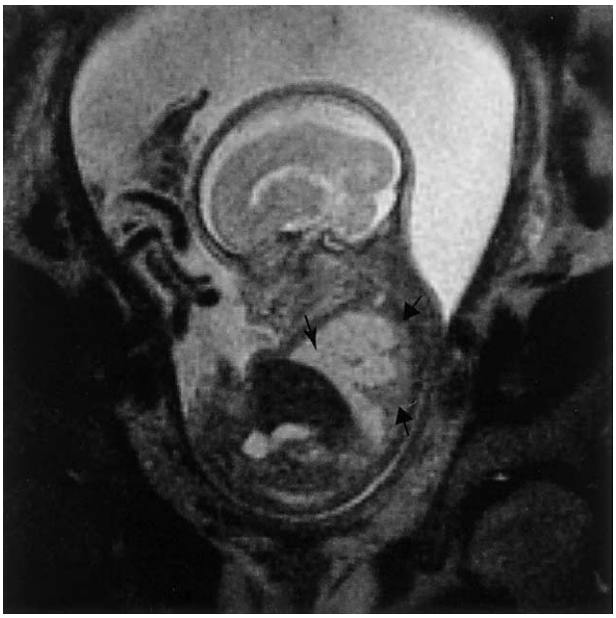

Fig 14. Cystic adenomatoid malformation of a lung in a fetus at 20 weeks' gestation. Sagittal T_2-weighted image shows a large homogeneous high-signal-intensity mass (curved arrowhead) in the right chest with irregular margins that do not conform to lobar anatomy. Compressed remaining normal lung is seen posteriorly (large arrows).

cystic lesions are homogeneous and high signal intensity compared with the normal lung (Fig 13). With increasing numbers of micro- or macrocysts, the signal intensity increases, and the lesion becomes more heterogeneous. Discrete cysts are seen with MRI. MRI better shows normal compressed lung tissue than US. CCAM may arise from any segment or lobe of the lung and may involve multiple lobes (Fig 14).

The natural history of CCAM is variable. These lesions may decrease in size or appear to involute on prenatal US in 15% to 30% of cases. In one study of infants with prenatal involution of a CCAM, the postnatal CT showed lung cysts or focal lobar hyperinflation in 22 of 23.[35] Hydrops may occur in up to 40% of fetuses with CCAM. Lesions with large cysts have a high incidence of hydrops. Large tumors associated with hydrops and a dominant cyst may be treated with thoracoamniotic shunting.

A BPS is a mass of nonfunctioning pulmonary tissue that lacks connection to the tracheobronchial tree. BPS detected prenatally usually is extralobar. Sequestrations receive blood supply from a systemic artery. Although intralobar BPS are most common in the posterior segment of the left lower lobe, they may occur in any segment or lobe.[36] BPS may be associated with other anomalies including CDH, anomalous pulmonary venous drainage, pulmonary hypoplasia with Scimitar syndrome, bronchogenic cyst, bronchial esophageal connection, and horseshoe lung. Pulmonary sequestrations are a subgroup of lung lesion with a favorable prognosis.[37] Hydrops is uncommon unless there is an associated pleural effusion. On prenatal MRI, a BPS is a wedged-shaped area of high homogeneous signal (Fig 15).[32] US better shows anomalous systemic vessels with real-time color flow imaging. BPS may occur in the upper abdomen and be confused with an adrenal tumor. Although BPS in the chest is usually solid and homogeneous, in the upper abdomen it is usually cystic in the area of the adrenal gland and may be confused with neuroblastoma.[38]

Multiple chest lesions may be found simultaneously. Although chest lesions such as CCAM, BPS, and bronchogenic cyst used to be thought of as distinct lesions, there is significant overlap in their pathologic occurrence suggesting a similar embryologic development.[38] The most common is a hybrid lesion with US, MRI, and pathologic characteristics of CCAM, BPS, and systemic arterial blood supply.[39]

Congenital diaphragmatic hernia (CDH) represents a failure of formation of the diaphragmatic leaflets, occurring most commonly in the posterior aspect of the left diaphragm. They occur on the left, 88%; right, 10%; and bilateral, 2%. Survival rates in fetuses with CDH range from 40% to 90%.[41] Survival is related to the degree of pulmonary hypoplasia associated with the CDH. The

Fig 15. Bronchopulmonary sequestration in a fetus at 22 weeks' gestation. Axial T_2-weighted image shows a well-defined homogeneous high-signal-intensity mass (curved arrowhead) in the right lower lobe. There is a small feeding vessel (small arrow) arising from the descending aorta. Note the difference in signal intensity of the normal lung (double arrow).

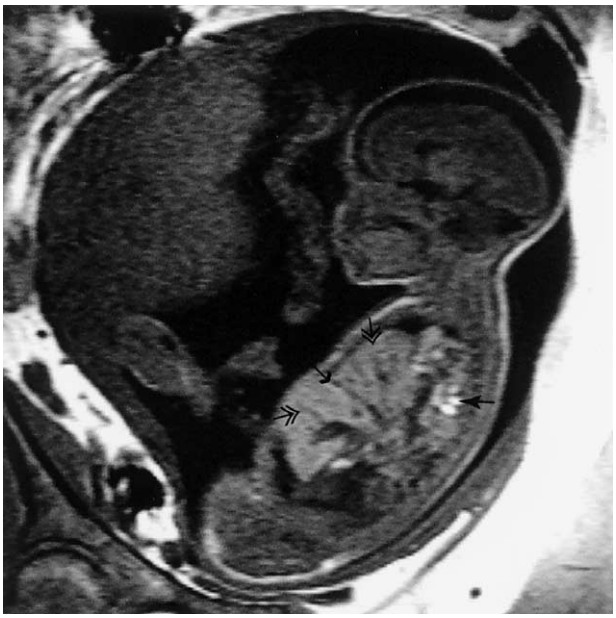

Fig 16. Congenital diaphragmatic hernia in a fetus 23 at weeks' gestation. Sagittal T_1-weighted image shows the high-signal-intensity liver (double arrows) above and below the remaining anterior diaphragmatic leaflet (small arrow). High-signal-intensity meconium filled loops of bowel are seen in the posterior chest (curved arrowhead).

best prenatal predictor of outcome remains the lung-to-head circumference ratio (LHR) determined on US.[42] One study has shown a correlation between the lung volume determined on MRI and outcome of fetuses with isolated left CDH when it was adjusted for gestational age at delivery and birth weight.[43] An another study, the calculated MRI fetal lung volume was not predictive of outcome.[44] However, the percentage of liver herniation into the chest was predictive of outcome. CDH with herniation of liver into the chest is associated with a worse prognosis with a survival rate less than 50%.

On US, CDH is diagnosed by showing a shift of the heart away from the midline and an area of increased echogenicity in the base of the chest. The stomach usually is in the chest. In one study of patients with postnatal repair of CDH, the diagnosis had been missed on prenatal US in 50% of fetuses.[45] Determination of liver position on US depends on the depiction of the portal and hepatic veins above or below the diaphragm providing indirect information about the hepatic position. MRI provides direct visualization of the liver.[46] T_1-weighted images show a high-signal-intensity liver (Fig 16). The signal intensity of lung and liver is significantly different on T_1 and T_2-weighted images. MRI is more accurate than US in detecting liver herniation.[47] Meconium-filled bowel has very high signal intensity on T_1-weighted images. MRI is most helpful in evaluation of right CDH. Right CDH is more frequently confused with CCAM because the stomach remains in the left upper quadrant of the abdomen.[47] The diagnosis of bilateral CDH is missed easily and may be difficult to make on US. The diagnosis is definitively made on MRI by demonstration of liver in the right chest and bowel in the left chest.

MRI is most useful for evaluating atypical chest masses.[32] A foregut cyst on MRI is a fluid-filled cyst with high, homogeneous signal.[48] The cyst may be large, and there may be a connection to vertebrae and associated vertebral body anomalies.

Anterior mediastinal masses are uncommon in utero. Fetal mediastinal teratoma has been reported.[49] On US these are complex cystic and solid masses. Because they are unusual lesions, they may be misdiagnosed as CCAM. MRI confirms the tumor characteristics and relationship to the trachea and vessels in the thoracic inlet and superior mediastinum. Lymphangiomas may occur anywhere in the body. Lymphangioma is more likely to violate tissue planes. They appear as complex cystic masses with a variable solid component. Any chest mass may be associated with hydrops if there is obstruction of venous return.

ABDOMEN

The fetal liver is well visualized on prenatal MRI. Physiologic changes have been seen within the fetal liver using echo-planar imaging (EPI).[50] Iron causes attenuation of the signal on EPI and T_2-weighted images. Early in fetal life, the majority of erythropoiesis occurs in the liver; consequently, there is a large amount of iron bound to fetal hemoglobin in the liver. There is a large change in the distribution of erythropoiesis, between 20 and 26 weeks gestation. Changes in signal intensity of the liver can be seen throughout fetal development. Changes in T_2* measurements of the fetal liver have been documented after maternal oxygenation based on the blood oxygenation level dependence (BOLD) of the MRI signal.[51] This technique may help evaluate abnormalities such as placental insufficiency and intrauterine growth retardation.

Fetal bowel is visualized on prenatal MRI.[46] Meconium is seen in the rectum on MRI as early as 14 weeks gestation. Meconium is seen in the mid-to distal bowel in all fetuses with normal bowel. If meconium is not seen, atresia or perforation should be suspected. On T_2-weighted images the stomach and proximal bowel are high in signal, similar to amniotic fluid, and the distal bowel is low in signal intensity. MRI differentiates abnormalities such as bowel obstruction from other cystic masses in the abdomen. MRI shows the site of bowel atresia.[52]

Abdominal masses can be detected with prenatal MRI (Fig 17).[53] An abdominal mass may be associated with

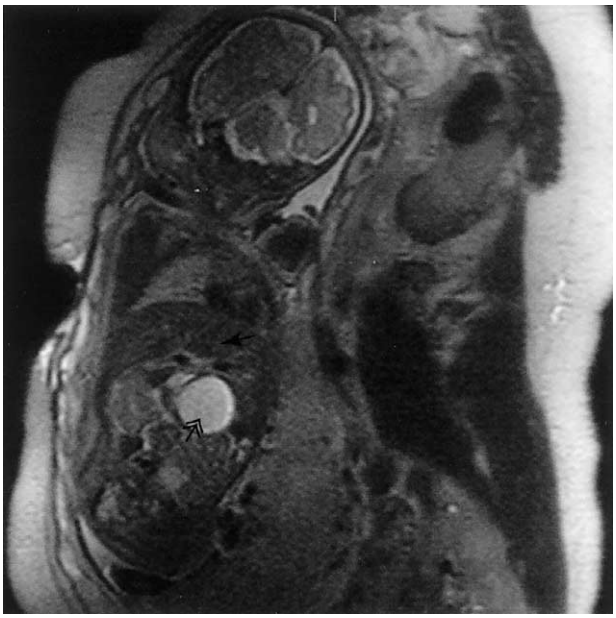

Fig 17. Duodenal duplication cyst in a fetus at 27 weeks' gestation. Coronal T_2-weighted image shows a large well-defined high-signal-intensity cystic mass (double arrow) in the upper abdomen. The liver (curved arrowhead) is normal in size and signal intensity and dilation of the bile ducts.

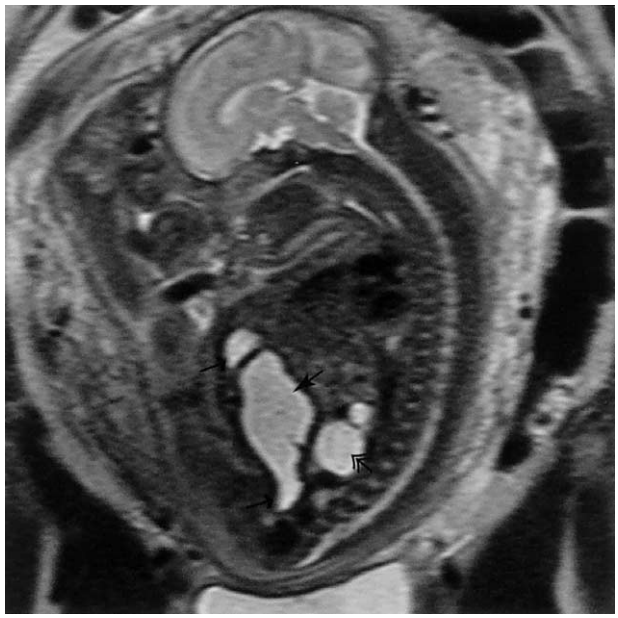

Fig 18. Lower urinary tract obstruction in a fetus at 26 weeks' gestation. Sagittal T_2-weighted image shows an enlarged thick walled urinary bladder (curved arrowhead) with dilation of the posterior urethra, a persistent urachus (small arrow), and severe dilation of the ureter (double arrow). There is severe oligohydramnios.

polyhydramnios secondary to compression of the bowel. Liver tumors are rare in the fetus, although hemangioendotheliomas, hepatoblastomas, and hamartomas do occur. Hemangioendotheliomas are mixed in intensity depending on the size of the vascular pools and the degree of fibrosis. Hepatomegaly usually is present. Hamartomas typically are irregular cystic masses. Calcifications may be present. Hepatomegaly may be seen also with hydrops, infection, anemia, metabolic abnormalities, and Beckwith-Wiedemann syndrome.

Neuroblastoma (NBL) is one of the more common solid childhood tumors.[54] There are few reports of NBL diagnosed in utero. Fetal neuroblastomas are cystic, which is uncommon in NBL diagnosed after birth. Congenital renal masses are rare, but mesoblastic nephroma has been diagnosed in utero.[54] These are predominantly solid masses but may contain cysts. There may be hemorrhage in areas of tumor necrosis.

Fetal renal anomalies often are associated with oligohydramnios, a condition that may make the performance of US difficult. The performance of MRI is not significantly affected by diminished amniotic fluid. The normal fetal kidney is intermediate in signal intensity on T_2-weighted images. The signal of the cortex is slightly lower than the medulla. The renal pelves and bladder have very high signal intensity on T_2-weighted images.[55]

Renal anomalies are increasingly detected with US because of significant improvements in technology. It is

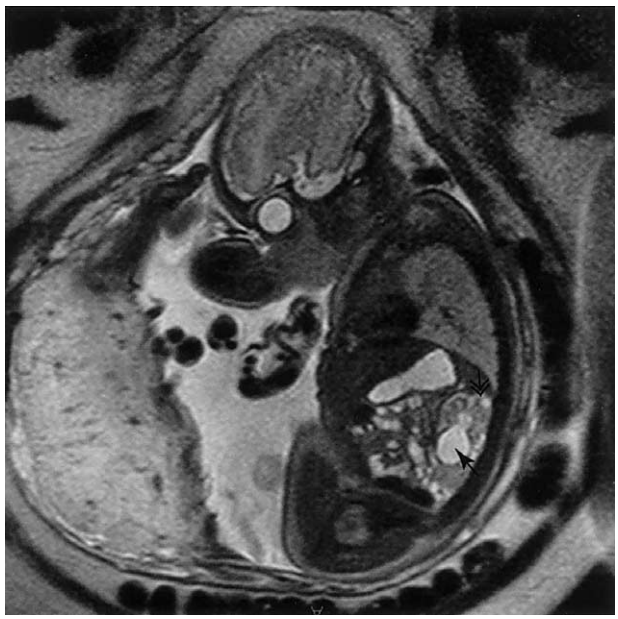

Fig 19. Lower urinary tract obstruction in a fetus at 28 weeks' gestation. Sagittal T_2-weighted imaged shows moderate dilation of the renal pelvis (curved arrowhead). The renal cortex is inhomogeneous with discrete cysts (double arrow) consistent with dysplastic changes.

estimated that 1 in 1,000 fetuses have a renal anomaly.[56] The mortality rate after antenatal detection of fetal uropathy ranges from 20% to 50%.[57] Associated anomalies have been found in 50% of fetuses.[57] The urinary bladder is dilated and thick walled with uropathy caused by lower urinary tract obstruction (LUTO; Fig 18). MRI is equal to US in the accuracy of identifying a LUTO but is no better at differentiating the causes, such as posterior urethral valves, urethral atresia, and prune belly syndrome. With progressive obstruction of the bladder there is associated dilation of one or both renal collecting systems. Renal dysplastic changes occur with progressive dilation of the renal tubules, which become cysts in the cortex and medulla. Renal dysplastic changes are seen as patchy areas of increased signal intensity throughout the cortex or cysts. MRI helps determine whether cortical abnormalities are dysplastic changes or normal cortical variants.[55] (Fig 19). The presence of renal dysplasia associated with a urinary tract obstruction is a poor prognostic sign and is associated with markedly decreased renal function. MRI defines the anatomy of complex renal anomalies, such as bladder extrophy and cloacal anomalies.[55] The ability to define the bowel and the urinary tract helps distinguish these from other forms of LUTO.

Improvements in MRI technology yield faster scan times and higher resolution increasing the applications for fetal imaging. MRI is an adjunct to good prenatal US. It provides significant additional information that improves diagnostic accuracy.

REFERENCES

1. Quinn T, Hubbard A, Adzick N: Prenatal magnetic resonance imaging enhances fetal diagnosis. J Pediatr Surgery 33:553-338, 1998
2. Levine D, Barnes P, Sher S, et al: Fetal fast MR imaging: Reproducibility, technical quality, and conspicuity of anatomy. Radiology 206:549-554, 1998
3. O'Connor M: Intrauterine effects in animals exposed to radiofrequency and microwave fields. Teratology 59:287-291, 1999
4. Myers C, Duncan K, Gowland P, et al: Failure to detect intrauterine growth restriction following in utero exposure to MRI. Br J Radiol 71:549-551, 1998
5. Baker P, Johnson I, Harvey P, et al: A three-year follow-up of children imaged in utero with echo-planar magnetic resonance. Am J Obstet Gynecol 170:32-39, 1994
6. Levine D, Barnes P, Madsen J, et al: Central nervous system abnormalities, assessed with prenatal magnetic resonance imaging. Obstet Gynecol 94:1011-1019, 1999
7. Simon E, Goldstein R, Coakley F, et al: Fast MR imaging of fetal CNS anomalies in utero. Am J Neuroradiol 21:1688-1698, 2000
8. Brisse H, Fallet C, Sebag G, et al: Supratentorial parenchyma in the developing fetal brain: In vitro MR study with histologic comparison. Am J Neuroradiol 8:1491-1497, 1997
9. Garel C, Chantrel E, Brisse H, et al: Fetal cerebral cortex: Normal gestational landmarks identified using prenatal MR imaging. Am J Neuroradiol 22:184-189, 2001
10. Lan M, Yamashita Y, Tang T, et al: Normal fetal brain development: MR imaging with a half-fourier rapid acquisition with relaxation enhancement sequence. Radiology 15:205-210, 2000
11. Girard N, Raybaud C, Ponce M, et al: In vivo MR study of brain maturation in normal fetuses. Am J Neuroradiolo 16:407-413, 1995
12. Levine D, Barnes P: Cortical maturation in normal and abnormal fetuses as assessed with prenatal MR imaging. Radiology 210:751-758, 1999
13. Barkovich A, Rowley H, Bollen A, et al: Correlation of prenatal events with the development of polymicrogyria. Am J Neuroradiol 16:822-827, 1995
14. Sonigo P, Rypens F, Carteret M, et al: MR imaging of fetal cerebral anomalies. Pediatri Radiol 28:212-222, 1998
15. Denis D, Maugey-Laulom B, Carles D, et al: Prenatal diagnosis of schizencephaly by fetal magnetic resonance imaging. Fetal Diagn Ther 16:354-359, 2001
16. Nyberg D, Mack L, Hirsch J, et al: Fetal hydrocephalus: Sonographic detection and clinical significance of associated anomalies. Radiology 163:187-191, 1987
17. Oi S, Honda Y, Hidaka M, et al: Intrauterine high-resolution magnetic resonance imaging in fetal hydrocephalus and prenatal estimation of postnatal outcomes with "perspective classification." J Neurosurg 88:685-694, 1998
18. Toma P, Lucigrai G, Ravegnani M, et al: Hydrocephalus and porencephaly: Prenatal diagnosis by ultrasonography and MR imaging. Comput Assist Tomograph 14:843-845, 1990
19. Low JA, Simpson LL, Ramsey DA: The clinical diagnosis of asphyxia responsible for brain damage in the human fetus. Am J Obstet Gynecol 167:11-15, 1992
20. de Laveaucoupet J, Audibert F, Guis F, et al: Fetal magnetic resonance imaging (MRI) of ischemic/ hemorrhagic brain injury. Prenat Diagn 21:729-734, 2001
21. Toma P, Costa A, Magnano G, et al: Holoprosencephaly: Prenatal diagnosis by sonography and magnetic resonance imaging. Prenat Diagn 10:429-436, 1990
22. Levine D, Barnes P, Korf B, et al: Tuberous sclerosis in the fetus: Second-trimester diagnosis of subependymal tubers with ultrafast MR imaging. Am J Roentgenol 175:1067-1069, 2000
23. Stazzone M, Hubbard A, Bilaniuk L, et al: Ultrafast MR Imaging of the normal posterior fossa in fetuses. Am J Roentgenol 175:835-839, 2000
24. Nakahara T, Uozumi T, Monden S, et al: Prenatal diagnosis of open spina bifida by MRI and ultrasonography. Brain Devel 15:75-78, 1993
25. Mangels KJ, Tulipan N, Tsao LY, et al: Fetal MRI in the evaluation of intrauterine myelomeningocele. Pediatric Neurosurg 32: 123-131, 2000
26. Sutton L, Adzick N, Bilaniuk L, et al: Improvement in hindbrain herniation demonstrated by serial fetal MRI following fetal surgery for myelomeningocele. JAMA 282:1626-1831, 1999
27. Altman RP, Randolph JG, Lilly JR: Sacrococcygeal teratoma: American Academy of Pediatric Surgical Section Survey. J Pediatr Surg 9:389-398, 1974
28. Westerburg B, Feldstein V, Sandberg PL, et al: Sonographic prognostic factors in fetuses with sacrococcygeal teratoma. J Pediatr Surg 35:322-326, 2000
29. Avni FE, Guibaud L, Robert Y, et al: MR imaging of fetal sacrococcygeal teratoma: Diagnosis and assessment. Am J Roentgenol 78:179-183, 2002
30. Hubbard AM, Crombleholme T, Adzick NS: Prenatal MRI evaluation of giant neck masses in preparation for fetal exit procedure. Am J Perinatol 15:253-257, 1998

31. Tsuda H, Matsumoto M, Yamamoto K, et al: Usefulness of ultrasonography and magnetic resonance imaging for prenatal diagnosis of fetal teratoma of the neck. J Clinical Ultrasound 4:217-219, 1996

32. Hubbard AM, Adzick NS, Crombleholme TM, et al: Congenital chest lesions: Diagnosis and characterization with prenatal MR imaging. Radiology 212:43-48, 1999

33. Duncan K, Gowland P, Moore R, et al: Assessment of fetal lung growth in utero with echo planar MR imaging. Radiology 210:197-200, 1999

34. Duncan K, Gowland P, Freeman A, et al: The changes in magnetic resonance properties of the fetal lungs: A first result and a potential tool for the non-invasive in utero demonstration of fetal lung maturation. Br J Obstet Gynecol 106:122-125, 1999

35. Blau H, Barak A, Karmazyn B, et al: Postnatal management of resolving fetal lung lesions. Pediatrics 109:105-108, 2002

36. John PR, Beasley SW, Mayne V: Pulmonary sequestration and related congenital disorders. Pediatr Radiol 20:4-9, 1998

37. Bratu I, Flageole H, Chen MF, et al: The multiple facets of pulmonary sequestration. J Pediatr Surg 36:784-790, 2001

38. Pumberger W, Moroder W, Weisbauer P: Intraabdominal extralobar pulmonary sequestration exhibiting cystic adenomatoid malformation: Prenatal diagnosis and characterization of a left suprarenal mass in the newborn. Abdom Imaging 26:28-31, 2001

39. MacKenzie TC, Guttenberg ME, Nisenbaum HL, et al: A fetal lung lesion consisting of bronchogenic cyst, bronchopulmonary sequestration, and congenital cystic adenomatoid malformation: the missing link? Fetal Diagn Ther 16:193-195, 2001

40. Cass DL, Crombleholme TM, Howell LJ, et al: Cystic lung lesions with systemic arterial blood supply: A hybrid of congenital cystic adenomatoid malformation and bronchopulmonary sequestration. J Pediatr Surg 7:986-990, 1997

41. Harrison M, Adzick N, Estes J, et al: A prospective study of the outcome of fetuses with diaphragmatic hernia. J Am Med Assoc 271:382-384, 1994

42. Sbragia L, Paek B, Filly R, et al: Congenital diaphragmatic hernia without herniation of the liver: Does the lung-to-head ratio predict survival? J Ultrasound Med 19:845-848, 2000

43. Paek BW, Coakley FV, Lu Y, et al: Congenital diaphragmatic hernia: Prenatal evaluation with MR lung volumetry—Preliminary experience. Radiology 220:63-67, 2001

44. Walsh DS, Hubbard AM, Olutoye OO, et al: Assessment of fetal lung volumes and liver herniation with magnetic resonance imaging in congenital diaphragmatic hernia. Am J Obstet Gynecol 183:1067-1069, 2000

45. Lewis DA, Reickert C, Bowerman R, et al: Prenatal ultrasonography frequently fails to diagnose congenital diaphragmatic hernia. J Pediatr Surg 32:352-356, 1997

46. Hubbard A, Adzick N, Crombleholme T, et al: Left sided congenital diaphragmatic hernia: Value of prenatal MR imaging in preparation for fetal surgery. Radiology 203:636-640, 1997

47. Hubbard AM, Crombleholme T, Adzick N, et al: Prenatal MRI of congenital diaphragmatic hernia. Am J Perinatol 16:407-413, 1999

48. Gulrajani M, David K, Sy W, et al: Prenatal diagnosis of a neuroenteric cyst by magnetic resonance imaging. Am J Perinatol 18:304-306, 1993

49. Wang RM, Shih JC, Ko TM: Prenatal sonographic depiction of fetal mediastinal immature teratoma. J Ultrasound Med 19:289-295, 2000

50. Duncan K, Baker P, Gowland P, et al: Demonstration of changes in fetal liver erythropoiesis using echo-planar magnetic resonance imaging. Am J Physiol 273:965-967, 1997

51. Semple SI, Wallis F, Haggarty P, et al: The measurement of fetal liver T2* in utero before and after maternal oxygen breathing: Progress towards a non-invasive measurement of fetal oxygenation and placental function. Magn Reson Imaging 19:921-928, 2001

52. Benachi A, Nigo P, Jouannic JM, et al: Determination of anatomical location of an antenatal intestinal occlusion by magnetic resonance imaging. Ultrasound Obstet Gynecol 18:163-165, 2001

53. Toma P, Lucigrai G, Dodero P, et al: Prenatal detection of abdominal mass by MR imaging performed while the fetus is immobilized with pancuronium bromide. Am J Roentgenol 154:1049-1050, 1990

54. Garmel SH, Crombleholme TM, Semple JP, et al: Prenatal diagnosis and management of fetal tumors. Semin Perinatol 18:350-365, 1994

55. Hubbard A, Harty M, Ruchelli E, et al: Prenatal MRI of the fetal urinary tract: Normal and abnormal anatomy with US and pathologic correlation. Radiology 209S:259, 1998

56. Estes J, Harrison M: Fetal obstructive uropathy. Semin Pediatr Surg 2:129-135, 1993

57. Cusick E, Didier F, Droulle P, et al: Mortality after an antenatal diagnosis of fetal uropathy. J Pediatr Surg 30:463-466, 1995